J Mol Model (2013) 19:1167–1177
DOI 10.1007/s00894-012-1653-3

ORIGINAL PAPER

Molecular dynamics and free energy studies of chirality specificity effects on aminobenzo[a]quinolizine inhibitors binding to DPP-IV

Cui Wei · Liang Desheng · Gao Jian · Luo Fang · Geng Lingling · Ji Mingjuan

Received: 3 August 2012 / Accepted: 15 October 2012 / Published online: 15 November 2012

Abstract The aminobenzo[a]quinolizines were investigated as a novel class of DPP-IV inhibitors. The stereochemistry of this class plays an important role in the bioactivity. In this study, the mechanisms of how different configuration of three chiral centers of this class influences the binding affinity were investigated by molecular dynamics simulations, free energy decomposition analysis. The S configuration for chiral center 3* is decisive for isomers to maintain high bioactivity; the chirality effect of chiral center 2* on the binding affinity is largely dependent, while the S configuration for chiral center 2* is preferable to R configuration for the bioactivity gain; the effect of chiral center 11b* on the binding affinity is insignificant. The chirality specificity for three chiral centers is responsible for distinction of two van der Waals contacts with Tyr547 and Phe357, and of H-bonding interactions with Arg125 and Glu206. Particularly, the Arg125 to act as a bridge in the H-bonding network contributes to stable H-bonding interactions of isomer in DPP-IV active site.

Keywords Aminobenzo[a]quinolizine inhibitors · Chirality specificity · DPP-IV · MM/GBSA · Molecular dynamics simulations

Cui Wei and Liang Desheng contributed equally to this work.

Electronic supplementary material The online version of this article (doi:10.1007/s00894-012-1653-3) contains supplementary material, which is available to authorized users.

C. Wei · L. Desheng · G. Jian · L. Fang · G. Lingling · J. Mingjuan (✉)
College of Chemistry and Chemical Engineering,
Graduate University of the Chinese Academy of Sciences,
Beijing 100049, People's Republic of China
e-mail: kejianjmj@gmail.com

Introduction

Type II diabetes is a chronic, progressive metabolic disease with abnormal insulin secretion caused by impaired islet β-cell function and insulin resistance in target issue [1, 2]. Dipeptidyl peptidase IV (DPP-IV) inhibitors have proved to be a new therapeutic option with novel mechanisms of action and improved tolerability [3–5]. DPP-IV is a ubiquitous serine protease responsible for the cleavage and inactivation of the incretin hormones glucagons like peptide-1 (GLP-1) and glucose dependent insulintropic polypeptide (GIP). Both of GLP-1 and GIP are potent stimulators of endogenous insulin release and have favorable effects on the islet β-cell function and insulin selectivity. Inhibition of DPP-IV could prolong the half life of GLP-1 and GIP, as well as stabilize the beneficial efficacy of the incretin hormones [6–8]. Particularly, DPP-IV inhibitors have had rapid rise in popularity due to the excellent safety profiles (no hypoglycemia, no weight gain and no gastrointestinal problems, no typical side effects associated with other antidiabetic agents). As a result, it has brought about the international passion to develop the novel class of DPP-IV inhibitors in the last few years. Currently, several kinds of DPP-IV inhibitors have been advanced into late stage clinical studies. Among them, sitagliptin [9–11], vildagliptin [12, 13], and alogliptin [14, 15] have been approved and successfully launched in several countries.

The aminobenzo[a]quinolizine analogues identified via high-throughput screening (HTS) was a promising class of non-peptidomimetic inhibitors of DPP-IV that are structurally distinct [16, 17]. Experimental assays showed that the stereochemistry of this class has a major influence on the binding affinity. As shown in Fig. 1, the enantiomer SSS of compound 1 is potent with half

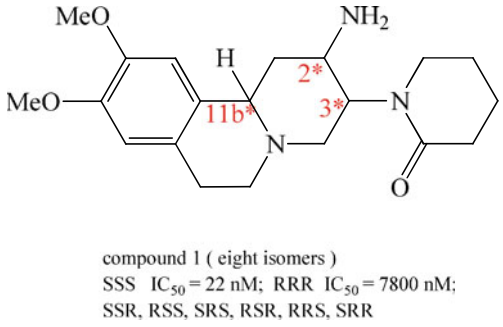

Fig. 1 The chemical structure with IC_{50} value of the aminobenzo[a] quinolizine inhibitor of DPP-IV (The three chiral centers are labeled as 2*, 3*, and 11b*, respectively, the eight isomers generated were listed as SSS, SSR, RSS, SRS, RSR, RRS, SRR, and RRR, respectively)

maximum inhibitory concentration (IC_{50}) value of 22 nM, whereas its enantiomer RRR is virtually inactive with IC_{50} of 7800 nM. Recently, the crystal structure of DPP-IV complex with the aminobenzo[a]quinolizine inhibitors was determined at the atomic level by the X-ray diffraction method [17].

Discussing how the different configuration of three chiral centers influences the binding affinity can help us understand the chirality specificity binding mechanisms of them with DPP-IV, and further provide some clues for optimizations and design of them. For this purpose, molecular dynamics (MD) simulations were used as a powerfully computational strategy. Currently, several optional methods have been developed to predict binding free energy of protein-ligand complex, including linear interaction (LIE) [18, 19], free energy perturbation (FEP) [20], thermodynamic integration (TI) [21], and molecular mechanics/generalized Born surface area (MM/GBSA) method [22, 23]. In view of computational demand and precision, the MM/GBSA method is applied in this work, which includes the effect of thermal averaging with force field/continuum solvent models to postprocess a series of representative snapshots derived from molecular dynamics trajectories.

In this work, the concept of biological residues mutation was adopted to obtain eight isomers of compound 1 through mutating its three chiral centers. The related isomers were listed as SSS, SSR, RSS, SRS, RSR, RRS, SRR, and RRR respectively. Firstly the 2 ns molecular dynamics simulations were conducted for eight isomers in complex with DPP-IV, then MM/GBSA method was applied to evaluate the binding free energies of eight complexes, finally the MM/GBSA free energy decomposition analysis [24–26] was made to obtain the detailed information of inhibitor-residue pair based interactions. We sought to elucidate the molecular basis of chirality specificity binding mechanisms of the aminobenzo[a]quinolizine inhibitors with DPP-IV from the qualitative and quantitative perspective, respectively.

Materials and methods

Initial structures for MD simulations

The chemical structure of compound 1 and the experimental biological activity were reported from the previous work [17], and shown in Fig. 1. The crystal structure of DPP-IV complex (PDB entry: 3KWF at 2.4 Å resolution) was retrieved from the RCSB Protein Data Bank (PDB) [17]. The initial structure of isomer SSS of compound 1 was rebuilt by modifying the ligand in 3KWF, the primary amine group of which was protonated with +1.0 charges, while the other seven related isomers of compound 1 were constructed on a basis of the isomer SSS through mutating the chiral centers. The established eight isomers were first minimized and then docked into the active site of DPP-IV via *FlexX* program in the *Sybyl 7.1* platform [27]. In the docking process, the flexibility of the ligand was taken into account while the protein was treated as a rigid structure. The parameters in FlexX were set as default values and the ranked 50 conformations were collected for cluster analysis, which were then sorted into three clusters: cluster A (RMSD in 0~3 Å), cluster B (RMSD in 3~6 Å), cluster C (RMSD>6 Å) based on the root-mean-square-displacement (RMSD) values relative to the crystal structure, and the pose with the highest docking score in the dominant cluster for each isomer was finally selected as the optimal starting structure for MD simulations. All the MD simulation projects of the obtained eight DPP-IV complexes with isomers were carried out with AMBER 9.0 software package [28]. The standard AMBER force field for bioorganic systems (*ff03*) [29] was used for DPP-IV protein energy minimization and dynamics simulations, while the general AMBER force field (*gaff*) [30] was used for the isomers. Due to lack of electrostatic parameters of ligand in the *gaff* force field, all eight isomers were preprocessed with *Hartree-Fock/6-31 G** optimization in *Gaussian 03* program [31] to determine the electrostatic potentials, then the *RESP* fitting technique [32] in AMBER program was applied to converge the partial atomic charges of isomers. All eight complexes were finally immersed in a truncated octahedron periodic box saturated with TIP3P water molecules [33], and the water box is extended 12 Å away from any solute atoms. Finally, the counter-ions (Na^+ ions) were added to neutralize the whole solvent system by *Leap* program [28] in AMBER 9.0 package.

Molecular dynamics simulations

Prior to MD simulations, energy optimizations of eight DPP-IV complexes with isomers were performed with *Sander* program [28] according to three procedures. First, the water molecules and ions were relaxed while the protein restrained (2500 iterations for steepest descent algorithm and then 2500 iterations for conjugated gradient algorithm);

second, the side chains of the DPP-IV protein were relaxed with the backbone atoms of protein restrained (5000 steps of steepest descent and 5000 steps of conjugate gradient minimizations); finally, the entire solvent systems were optimized without any constraint (5000 steps of steepest descent and 5000 steps of conjugated gradient minimizations).

Then, the whole solvent systems gradually heated under the canonical ensemble from 0 K to 310 K over 60 ps, and the 2 ns MD simulations with 2 fs time step were performed at a constant temperature of 310 K by the *Weak-coupling* algorithm [34]. In MD simulations, the *SHAKE* algorithm [35] was used to constrain all bonds related to hydrogen atoms, while the particle mesh Ewald (*PME*) algorithm [36] was to deal with the long-range electrostatic interactions. During the sampling process, the coordinates were saved every 10 ps interval for further binding free energy calculation and free energy decomposition analysis.

MM/GBSA calculations of binding free energies

The binding free energy was calculated using MM/GBSA algorithm in accordance with the following equation [22, 23]:

$$\begin{aligned}\Delta G_{\text{bind}} &= G_{\text{complex}} - G_{\text{protein}} - G_{\text{ligand}} \\ &= \Delta E_{\text{MM}} + \Delta G_{\text{GB}} + \Delta G_{\text{SA}} - T\Delta S \\ &= \Delta E_{\text{vdw}} + \Delta E_{\text{ele}} + \Delta G_{\text{GB}} + \Delta G_{\text{SA}} - T\Delta S\end{aligned} \quad (1)$$

where ΔE_{MM} denotes the gas-phase interaction energy between protein and ligand (including van der Waals energy term ΔE_{vdw} and electrostatic energy term ΔE_{ele}); ΔG_{GB} and ΔG_{SA} indicate the polar and non-polar desolvation free energy, respectively; $-T\Delta S$ represents the entropy contribution at temperature T. The polar desolvation term ΔG_{GB} was determined by the generalized Born (*GB*) approximation model [37], while the non-polar desolvation term ΔG_{SA} was estimated on a basis of solvent-accessible surface area (*SASA*) model determined by *LCPO* method [38]: $\Delta G_{\text{SA}} = 0.0072 \times \Delta SASA$. In this work, due to the relatively high computational demand of prediction of entropy in AMBER 9.0, as well as the extremely time-consuming calculations for the large biological systems, the estimations of entropy contribution in the binding process were not performed for all eight complex systems. In this text, the relative values of binding free energies for the eight isomers concerned were carefully compared and analyzed to explore the different chirality specificity effects of the three chiral centers on the binding affinity. The protein-inhibitor binding free energies were calculated based on 160 snapshots extracted from 0.4 to 2 ns MD simulation trajectories.

Inhibitor-residue pairs interaction decomposition

The inhibitor-residue interaction spectra were generated with MM/GBSA decomposition analysis by *mm_pbsa* program in AMBER 9.0 [24]. The interaction energy of each inhibitor-residue pair includes three energy terms: van der Waals energy contribution (ΔE_{vdw}), electrostatic energy contribution (ΔE_{ele}), and the desolvation energy term ($\Delta G_{\text{desolvation}}$). The desolvation energy term $\Delta G_{\text{desolvation}}$ is comprised of the polar term (ΔG_{GB}) and the non-polar term (ΔG_{SA}). The equation is summarized as follows:

$$\Delta G_{\text{inhibitor-residue}} = \Delta E_{\text{vdw}} + \Delta E_{\text{ele}} + \Delta G_{\text{GB}} + \Delta G_{\text{SA}} \quad (2)$$

The ΔE_{vdw} and ΔE_{ele} energy terms were calculated by the *sander* program in AMBER 9.0 [28]. The ΔG_{GB} term was calculated by the generalized Born (*GB*) model developed by Onufriev et al. [37]. The non-polar desolvation energy term (ΔG_{SA}) was determined on a basis of SASA determined with the *ICOSA* method [38]. All the energy components were calculated using 160 snapshots extracted from the MD trajectories from 0.4 to 2 ns.

Results and discussion

Molecular docking and assessment of the stability of MD simulations

All 50 docking conformations obtained for each isomer were categorized into three clusters: cluster A (RMSD in 0~3 Å), cluster B (RMSD in 3~6 Å), cluster C (RMSD> 6 Å) based on the root-mean-square-displacement (RMSD) values relative to the crystal structure (in Table S1). It can be seen that for each isomer cluster A is favorable in both the counts of conformation and the averaged docking score. Thus, the pose with the lowest predicted binding free energies in cluster A for each isomer was selected as the optimal initial complex structure for MD simulations. To investigate the dynamic stability and the rationality of sampling strategy for eight complexes, the RMSD values of the protein backbone atoms were calculated on a basis of starting snapshots and shown in Fig. 2. The fluctuation of RMSD values reveals that the conformations of eight complexes achieve equilibrium around 0.4 ns. The variations of the potential energies for eight complexes throughout 2 ns simulations were shown in Fig. 3. It can be noted that the potential energies of eight complexes remain stable after 0.4 ns. Thus, it is feasible to do the subsequent free energy calculations and free energy decomposition analysis based on the snapshots extracted from the MD trajectories from 0.4 ns to 2 ns.

Binding free energy predicted by MM/GBSA

To discern the differences of binding affinity of eight isomers with DPP-IV, the binding free energies of eight complexes were calculated by MM/GBSA method [22, 23]. The results of predicted binding free energies and energy

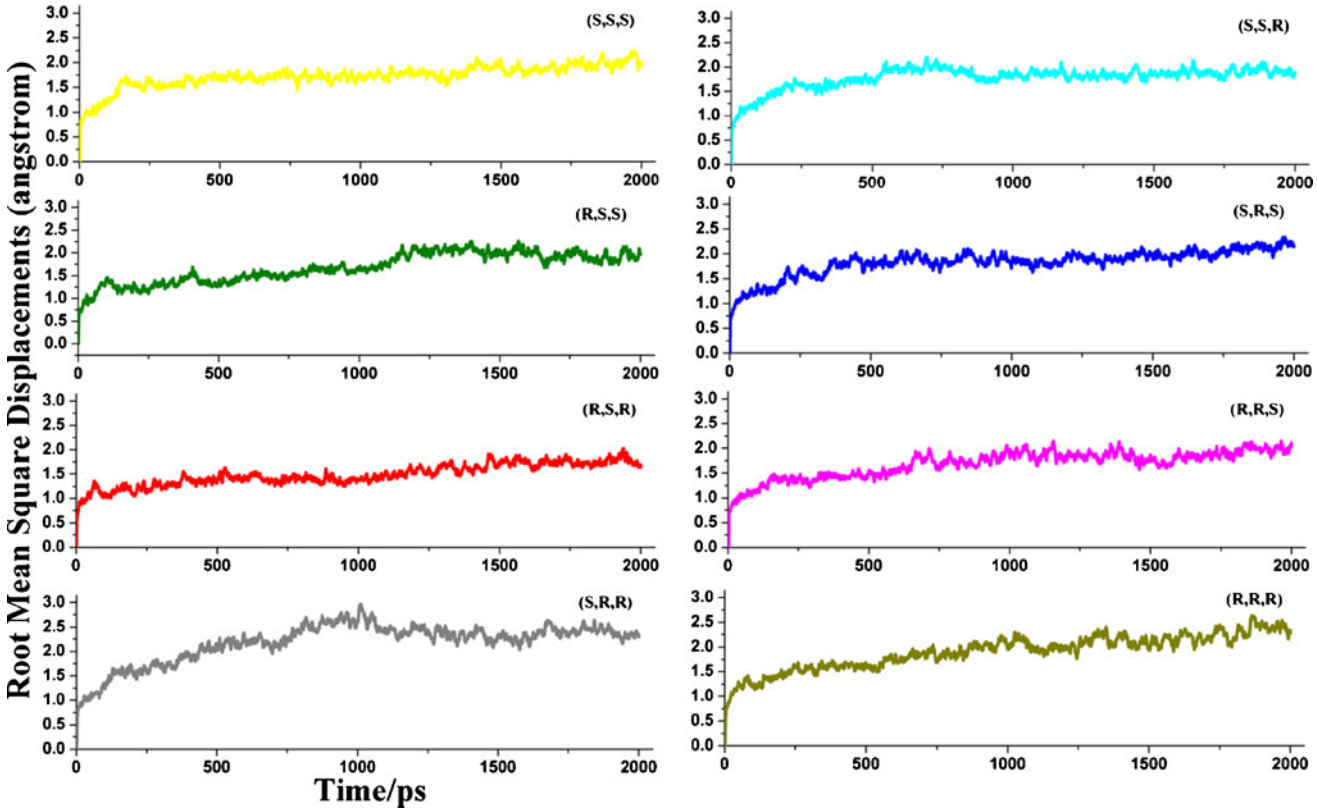

Fig. 2 RMSD of the backbone atoms of eight complexes with isomers versus 2 ns simulation time relative to their crystal structures

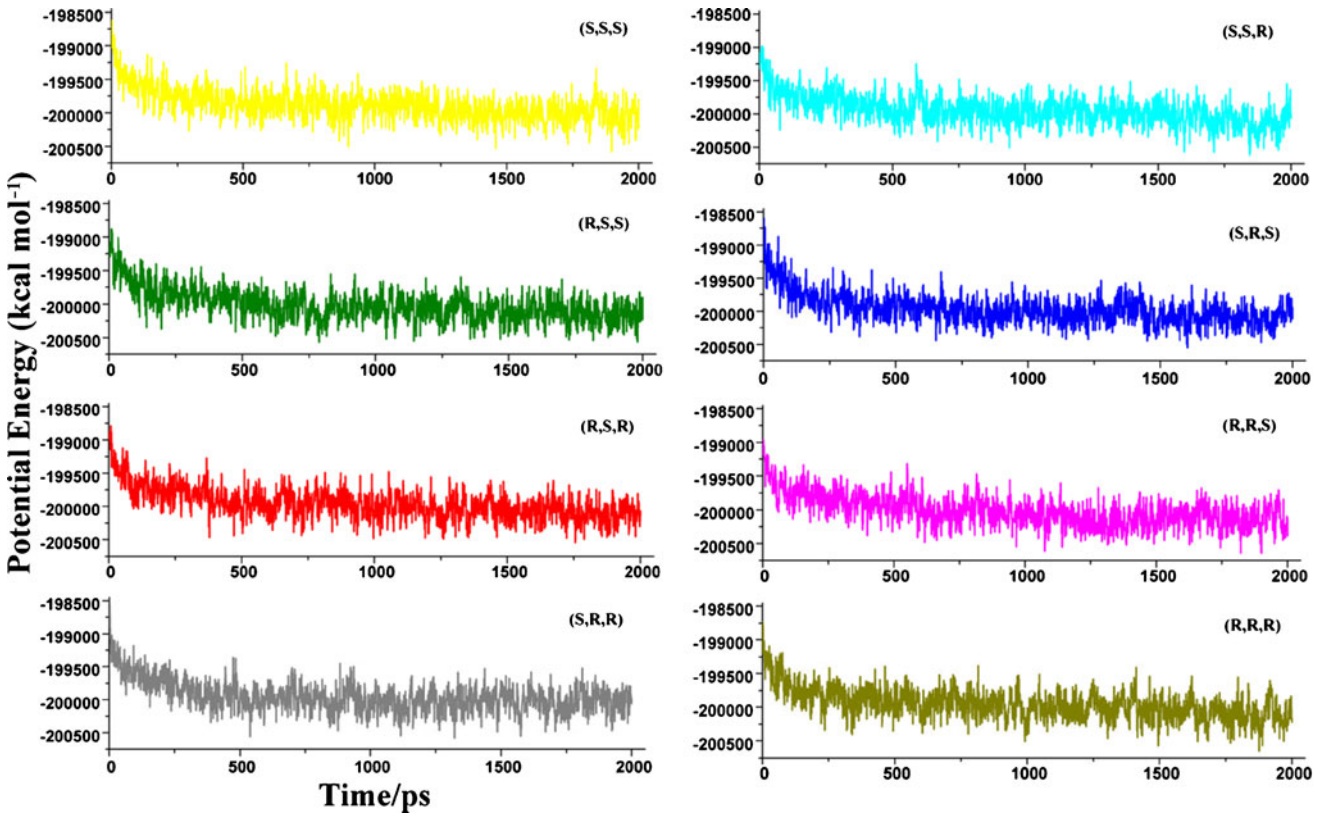

Fig. 3 Fluctuation of the potential energy of eight complexes with isomers versus 2 ns simulation time

components of eight complexes were summarized in Table 1. As indicated in Table 1, the IC_{50} values of enantiomer SSS and RRR are 22 and 7800 nM, respectively [17], that is, the pIC_{50} ($-\log IC_{50}$) values of two isomers are 7.66 and 5.11, respectively. The predicted binding free energies of enantiomer SSS and RRR are −29.23 and −8.76 kcal mol $^{-1}$, respectively. Thus, the predicted binding free energies of two isomers are consistent with the pIC_{50} values.

For better understanding which energy term has more impact on the binding affinity of eight isomers, the four individual energy components (ΔE_{vdw}, ΔE_{ele}, ΔG_{GB}, and ΔG_{SA}) listed in Table 1 were carefully compared. It can be noted that the van der Waals energy term (ΔE_{vdw}) dominates in the total binding free energy (ΔG_{pred}), and varies a lot among eight isomers. Of them, the ΔE_{vdw} of enantiomer SSS and RRR are −42.10 and −27.05 kcal mol $^{-1}$, respectively, which suggests significant difference between them. In comparison with the ΔE_{vdw} term, the gas phase electrostatic energy terms (ΔE_{ele}) encourage the binding affinity with much less contribution among eight isomers. Of them, the ΔE_{ele} of enantiomer SSS and RRR are −4.55 and −6.03 kcal mol $^{-1}$, respectively, which indicates no appreciable variation between them. However, the polar desolvation energy term (ΔG_{GB}) discourages the binding affinity to a large degree, and varies a lot among eight isomers. It is a surprise to note that there is no distinction between the ΔG_{GB} of the potent isomer SSS (+22.92 kcal mol $^{-1}$) and of the inactive isomer RRR (+28.73 kcal mol $^{-1}$). The negative penalty of the polar desolvation free energy (ΔG_{GB}) can not be fully offset by the gas phase electrostatic energy terms (ΔE_{ele}), so the net electrostatic contribution (ΔE_{ele}+ ΔG_{GB}) is still largely unfavorable for the binding affinity of eight isomers. The non-polar desolvation energy term (ΔG_{SA}) corresponding to the burial of solvent accessible surface area (SASA) slightly favor the binding affinity, and are nearly identical among eight isomers, which implies that all eight isomers can be better buried into the cavity of DPP-IV active site. Through the above analysis, it can be inferred that the van der Waals energy contributions and the unfavorable polar desolvation energy are the major reasons for the distinct binding affinity of eight isomers.

Analysis of the chirality effect on the binding affinity

To get a better view on how the R/S configuration of three chiral centers influences the binding affinity, the difference values of binding free energy ($\Delta\Delta G$) for diastereomer pairs were thoroughly investigated and the results were displayed in Fig. 4. As for chiral center 2* system, the eight isomers were divided into four diastereomer pairs according to chiral center 2* single mutation from S into R, which are (SSS-RSS), (SSR-RSR), (SRS-RRS), and (SRR-RRR), respectively. Similarly, the four diastereomer pairs for chiral center 3* single mutation from S into R are (SSS-SRS), (SSR-SRR), (RSS-RRS), and (RSR-RRR), respectively; while the four groups for chiral center 11b* single mutation from S into R are (SSS-SSR), (RSS-RSR), (SRS-SRR), and (RRS-RRR), respectively. In this part, we sought to discern the significance of chirality specificity of three chiral centers 3*, 2*, and 11b* to the binding affinity.

As shown in Fig. 4b is the distribution of $\Delta\Delta G$ for four diastereomer pairs for chiral center 3* single mutation from S into R, the $\Delta\Delta G$(SSS-SRS), $\Delta\Delta G$(SSR-SRR), $\Delta\Delta G$ (RSS-RRS), and $\Delta\Delta G$(RSR-RRR) are largely negative, which are −16.46, −4.26, −2.15, and −13.03 kcal mol $^{-1}$ respectively. As chiral center 3* mutates from S into R, the binding free energy of isomer declines to varying degree in accordance with the configurations of chiral centers 2* and 11b*, while the isomers with the same configuration of 2* and 11b* have a greater loss of binding free energy, which can be proved by $\Delta\Delta G$ (SSS-SRS) and $\Delta\Delta G$ (RSR-RRR) are much larger than $\Delta\Delta G$ (SSR-SRR) and $\Delta\Delta G$ (RSS-RRS). Generally, the four cases suggests that the chiral center 3* single mutation from S into R disfavors the binding affinity of isomer; the S configuration for chiral center 3* is superior to R configuration for isomer to maintain high bioactivity. From Fig. 4a, the $\Delta\Delta G$ for four diastereomer pairs derived from chiral center 2* single mutation from S into R, $\Delta\Delta G$ (SSS-RSS), $\Delta\Delta G$ (SSR-RSR), $\Delta\Delta G$ (SRS-RRS), and $\Delta\Delta G$ (SRR-RRR) are −11.94, −0.04, +2.37, and −8.81 kcal mol $^{-1}$, respectively. On the whole, the generated negative penalty to the binding affinity by chiral center 2* single mutation into R is lessened compared to Fig. 4b, while the

Table 1 Predicted binding free energies and individual energy terms of eight isomers in complex with DPP-IV (kcal mol $^{-1}$)

Inhibitor	ΔE_{vdw}	ΔE_{ele}	ΔG_{GB}	$\Delta E_{ele}+\Delta G_{GB}$	ΔG_{SA}	ΔG_{pred}
(SSS)	−42.10±2.17	−4.55±2.44	22.92±3.40	18.37±2.29	−5.50±0.14	−29.23±3.2
(SSR)	−43.24±2.28	−10.79±6.00	38.05±6.10	27.26±4.05	−5.85±0.11	−21.83±4.36
(RSS)	−34.31±2.53	−6.32±7.04	28.57±7.21	22.25±4.65	−5.23±0.26	−17.29±4.31
(SRS)	−35.46±3.20	−9.59±7.35	37.62±8.11	28.03±5.06	−5.34±0.26	−12.77±5.13
(RSR)	−37.67±3.16	−20.17±7.06	41.57±7.19	21.39±5.12	−5.52±0.19	−21.79±4.59
(RRS)	−34.85±2.53	−7.01±5.59	32.10±6.04	25.09±3.10	−5.38±0.30	−15.14±3.19
(SRR)	−35.48±3.55	−4.83±5.07	28.03±4.49	23.20±3.99	−5.28±0.27	−17.57±4.08
(RRR)	−27.05±2.22	−6.03±4.97	28.73±6.12	22.70±4.48	−4.41±0.42	−8.76±3.89

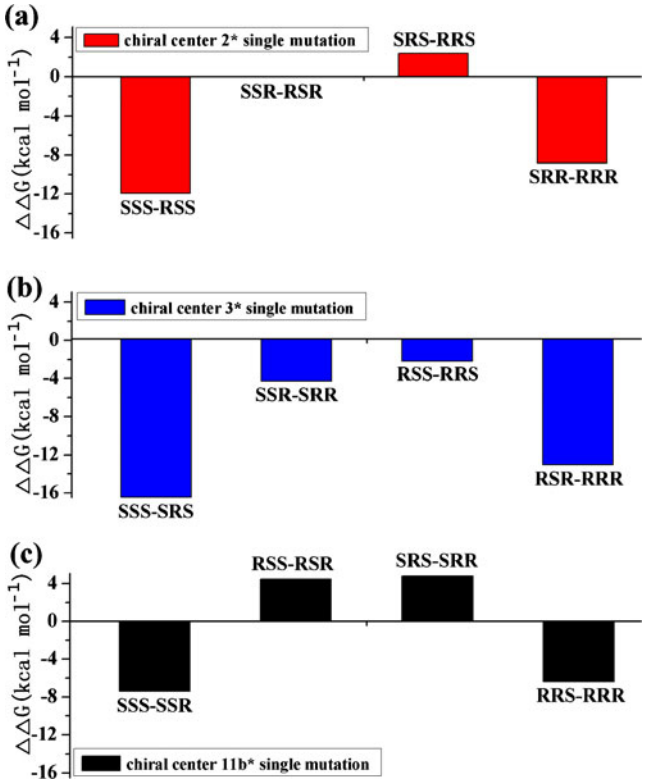

Fig. 4 The distribution of difference values of binding free energy ($\Delta\Delta G$) for the diastereomer pairs generated by chiral center single mutation from S into R, **a** $\Delta\Delta G$ for four diastereomer pairs for chiral center 2* single mutation from S into R; **b** $\Delta\Delta G$ for four diastereomer pairs for chiral center 3* single mutation from S into R; **c** $\Delta\Delta G$ for four diastereomer pairs for chiral center 11b* single mutation from S into R

same trend can be seen, the chiral center 2* single mutation into R leads to large reduction of binding free energy of isomer with the same configuration of chiral centers 3* and 11b*, while a slight change of binding free energy of isomer with different configuration of 3* and 11b*, which can be proved by the $\Delta\Delta G$ (SSS-RSS) and $\Delta\Delta G$ (SRR-RRR) are largely negative, the $\Delta\Delta G$ (SSR-RSR) and $\Delta\Delta G$ (SRS-RRS) are slightly negative or positive. From the four cases, it can be noted that the chirality effect of chiral center 2* on the binding affinity is largely dependent on chiral centers 3* and 11b*, while the S configuration for 2* is preferable to R configuration for the bioactivity gain. By comparison, in Fig. 4c, the $\Delta\Delta G$ for four diastereomer pairs generated by chiral center 11b* mutation from S into R, the $\Delta\Delta G$ (SSS-SSR), $\Delta\Delta G$ (RSS-RSR), $\Delta\Delta G$ (SRS-SRR), and $\Delta\Delta G$ (RRS-RRR) are −7.40, +4.50, +4.80, and −6.38 kcal mol $^{-1}$, respectively. During chiral center 11b* single mutation from S into R, the generated negative effect on the binding affinity declines a lot, while the positive effect on the binding affinity increases dramatically when compared to Fig. 4a and b. It is worth noting that the $\Delta\Delta G$ (SSS-SSR) and $\Delta\Delta G$ (RRS-RRR) demonstrate almost equivalent but utterly opposite tendency to the $\Delta\Delta G$ (RSS-RSR) and $\Delta\Delta G$ (SRS-SRR). As chiral center 11b* changes from S into R, the binding free energies of isomers SSS and RRS with the same configuration of chiral centers 2* and 3* are decreased, while those of isomers RSS and SRS with different configuration of chiral centers 2* and 3* are proportionally increased. The four cases indicates that the chirality specificity of chiral center 11b* to the binding affinity is insignificant, and is subject to the appreciable effect of chiral centers 2* and 3*. Additionally, the S configuration for 11b* displays no advantage to the bioactivity over the R configuration. Through the above analysis of three chiral centers, it can be inferred that the S configuration for chiral center 3* is decisive for isomer to maintain high bioactivity; the chirality effect of chiral center 2* on the binding affinity is largely dependent, while the S configuration for 2* is preferable to R configuration for the bioactivity gain; the chirality specificity for chiral center 11b* to the binding affinity is insignificant for the reason that it is subject to the appreciable mutual effect of chiral centers.

Decomposition analysis of difference values of binding free energies $\Delta\Delta G$

To further investigate the difference between binding modes of isomers, the MM/GBSA free energy decomposition analysis [24–26] was applied to decompose $\Delta\Delta G$ for diastereomer pairs, which helps to determine the key residues responsible for $\Delta\Delta G$, and to provide detailed information of binding modes of isomers on a basis of inhibitor-residue pair interactions. Here, it is worth mentioning that, as reported in previous work,[16, 17] the related residues in the binding of the aminobenzo[a]quinolizine inhibitors to DPP-IV active site mainly were Arg125, Glu205, Glu206, Phe357, Tyr547, Tyr631, Tyr662, Tyr666, and Asn710. Thus, we laid stress on the comparative analysis of difference values of interaction energy of these nine residues, and the cut-off value for the significant variance on the interaction energy was set to be ±1 kcal mol $^{-1}$.

The decomposition result of $\Delta\Delta G$ for four diastereomer pairs for chiral center 3* single mutation from S into R is illustrated in Fig. 5b. In $\Delta\Delta G$ (SSS-SRS), the variance of interaction energy of Phe357 (−1.31 kcal mol $^{-1}$) is beyond the cut-off value, which suggests the interaction of isomer with Phe357 declines a lot as isomer SSS mutates into SRS. On the other hand, the unfavorable polar desolvation energy increases dramatically (in Table 1, the ΔG_{GB} for isomer SSS and SRS are +22.92 and +37.62 kcal mol $^{-1}$, respectively). The variant interaction with Phe357, coupled with the different polar desolvation effects, could explain the distinct binding affinity of isomers SSS and of SRS. In $\Delta\Delta G$ (RSR-RRR), the change of isomer RSR into RRR greatly diminishes the interactions of isomer with Arg125 and Tyr547 (−2.05 and −1.16 kcal mol $^{-1}$). Thus, it is obvious to note

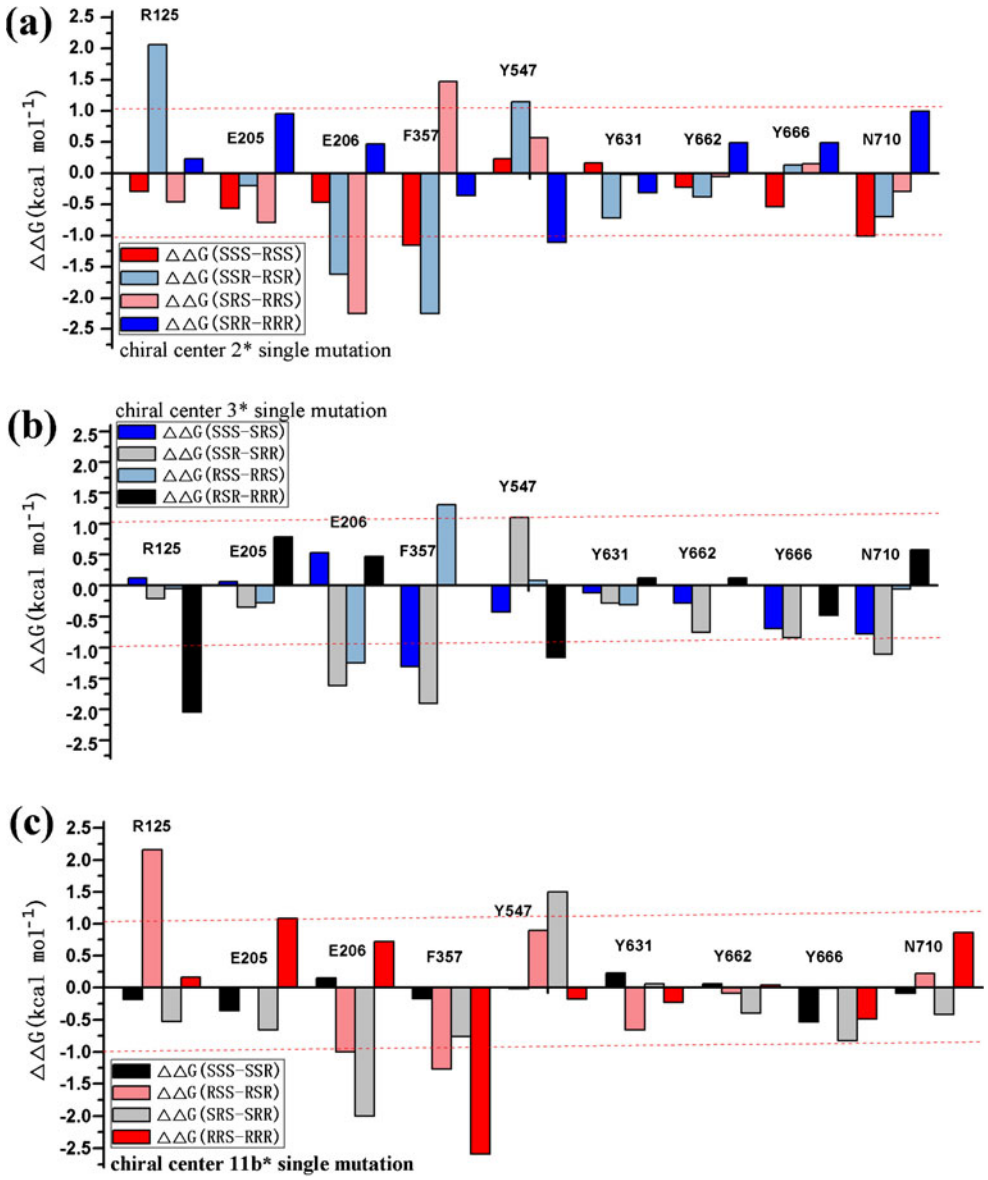

Fig. 5 The distribution of difference values of inhibitor-residue pair based interaction energy in decomposing $\Delta\Delta G$ for the diastereomer pairs generated by chiral center single mutation from S into R, **a** decomposition of $\Delta\Delta G$ for four diastereomer pairs for chiral center 2* single mutation from S into R; **b** decomposition of $\Delta\Delta G$ for four diastereomer pairs for chiral center 3* single mutation from S into R; **c** decomposition of $\Delta\Delta G$ for four diastereomer pairs for chiral center 11b* single mutation from S into R

that with chiral centers 2* and 11b* configured identically, the chiral center 3* single mutation from S into R is unfavorable for the interactions with residues. In $\Delta\Delta G$ (SSR-SRR), there is distinction between the binding modes of isomer SSR and of SRR, the change of isomer SSR into SRR greatly discourages the interactions of isomer with Glu206, Phe357, and Asn710 (−1.62, −1.90, and −1.11 kcal mol $^{-1}$, respectively), while it encourages the interaction with Tyr547 (+1.10 kcal mol $^{-1}$). In $\Delta\Delta G$ (RSS-RRS), the interaction of isomer with Glu206 (−1.25 kcal mol $^{-1}$) is greatly reduced, while the interaction with Phe357 (+1.31 kcal mol $^{-1}$) is strengthened as isomer RSS changes into RRS. Thus, it can be found that with chiral centers 2* and 11b* configured differently, generally, the chiral center 3* single mutation from S into R disfavors the interactions with residues, but induces improvements on individual interaction, which partly compensates for the generated negative penalty by the chiral center 3* single mutation into R. It could explain the fact $\Delta\Delta G$ (SSR-SRR) and $\Delta\Delta G$ (RSS-RRS) are much less than $\Delta\Delta G$ (SSS-SRS) and $\Delta\Delta G$ (RSR-RRR). To sum up the four cases for chiral center 3* single mutation system, it is clear to note that the chiral center 3* single mutation from S into R causes distinct interactions with Arg125, Glu206, Phe357, Tyr547, and Asn710.

In Fig. 5a, the interaction of isomer with Phe357 (−1.15 kcal mol $^{-1}$) declines greatly as isomer SSS mutates into RSS, while the interaction with Tyr547 (−1.11 kcal mol $^{-1}$) decreases a lot as isomer SRR mutates into RRR. It is obvious to see that with chiral centers 3* and 11b* configured identically, the chiral center 2* single mutation from S into R discourages the interactions of isomer with residues, but this generated negative effect tends to be lessened compared to Fig. 5b. In $\Delta\Delta G$ (SRS-RRS), the change of isomer SRS into RRS greatly diminishes the interaction with Glu206 (−2.25 kcal mol $^{-1}$), while it

greatly improves the interaction with Phe357 (+1.47 kcal mol $^{-1}$). In $\Delta\Delta G$ (SSR-RSR), there is distinction between the binding patterns of isomer SSR and of RSR, the isomer SSR mutation into RSR greatly weakens the interactions with Glu206 and Phe357 (−1.62 and −2.25 kcal mol $^{-1}$), but greatly strengthens the interactions with Arg125 and Tyr547 (+2.06 and +1.15 kcal mol $^{-1}$). In this mutation the positive effect on the interactions of isomer with residues is improved significantly and is almost equivalent to the negative penalty, which could explain the binding affinity of isomer SSR and of RSR being nearly identical. From the four cases for chiral center 2* system, it is revealed that the chiral center 2* single mutation from S into R causes distinct interactions with Arg125, Glu206, Phe357, and Tyr547. Compared to Fig. 5b, on the whole, the negative penalty to the interactions of isomer with residues caused by the chiral center 2* single mutation into R is lessened, while the favorable effect tends to be improved, and almost counterbalance the negative penalty.

As presented in Fig. 5c, there is no distinction between the binding modes of isomer SSS and of SSR, but the unfavorable polar desolvation energy increases dramatically as isomer SSS mutates into SSR (in Table 1, the ΔG_{GB} for isomer SSS and SSR are +22.92, and +38.05 kcal mol $^{-1}$, respectively), which could explain the variant binding affinity of isomer SSS and of SSR. In $\Delta\Delta G$ (RRS-RRR), the change of isomer RRS into RRR greatly discourages the interaction with Phe357 (−2.59 kcal mol $^{-1}$). In $\Delta\Delta G$ (SRS-SRR), the interaction of isomer with Glu206 (−2.00 kcal mol $^{-1}$) is lessened, while the interaction with Tyr547 (+1.50 kcal mol $^{-1}$) is strengthened as isomer SRS changes into SRR. In $\Delta\Delta G$ (RSS-RSR), the isomer RSS mutation into RSR weakens the interactions of isomer with Glu206 and Phe357 (−1.00 and −1.27 kcal mol $^{-1}$), but improved greatly the interaction with Arg125 (+2.16 kcal mol $^{-1}$). From the four cases for chiral center 11b* system, it is demonstrated that the chiral center 11b* single mutation from S into R induces distinct interactions with Arg125, Glu206, Phe357, and Tyr547. In comparison with Fig. 5a and b, the generated negative penalty to the interactions of isomer with residues by the chiral center 11b* single mutation into R is diminished obviously, while the positive effect is increased significantly, and even exceeds the negative penalty.

Based on the above analysis of three chiral centers, it can be inferred that the chirality specificity for three chiral centers is responsible for distinct interactions of isomer with Arg125, Glu206, Phe357, and Tyr547, which thus leads to variant binding modes of isomers with DPP-IV. From chiral centers 3*, 2* to 11b*, the generated negative penalty to the interactions of isomer with residues caused by chiral center single mutation into R is lessened, while the positive effect tends to be increased, and amounts to or even goes beyond the negative penalty, which confirms the variant significance of chirality effect of three chiral centers 3*, 2*, and 11b* on the binding affinity, consistent with the aforementioned inferences.

Analysis of binding modes of isomer SSS and RRR in complex with DPP-IV

The binding patterns of isomer SSS and isomer RRR in the active site were illustrated and carefully analyzed for better elucidation of the chirality specificity binding mechanisms of them with DPP-IV. In Fig. 6a, it can be observed that the caprolactam moiety of the potent isomer SSS nicely occupy

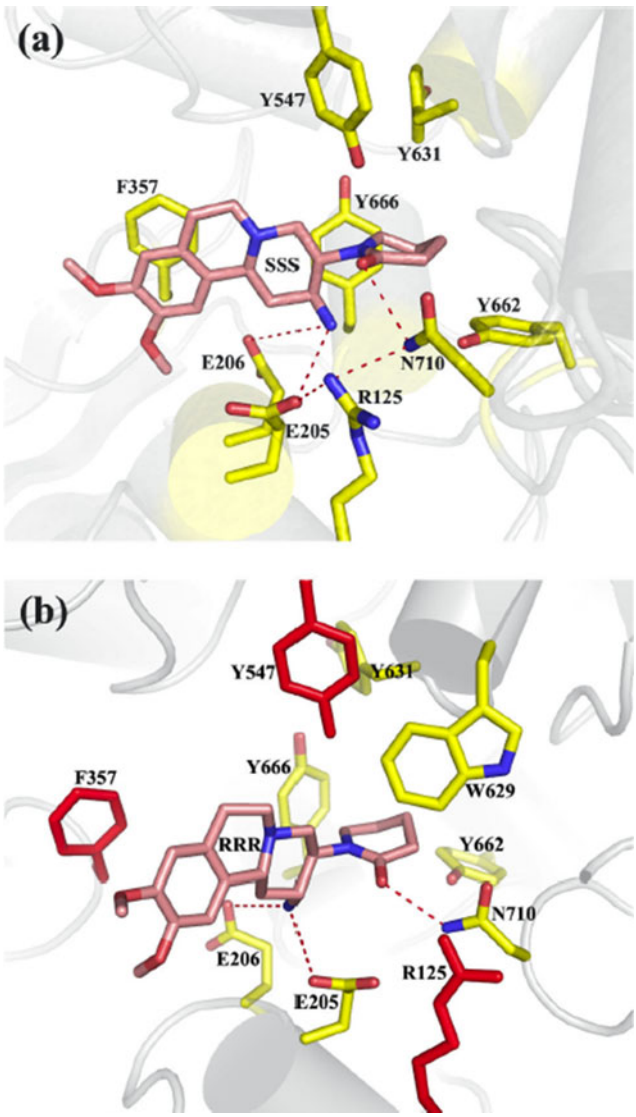

Fig. 6 Binding modes of isomer SSS and isomer RRR with the key residues of DPP-IV that are crucial for the binding affinity, **a** for isomer SSS, **b** for isomer RRR, the hydrogen bonds are represented by red dotted line; the isomers SSS and RRR shown as green stick representation are the lowest-energy structures obtained from MD simulations; the key residues are shown as yellow stick representation; the residues R125, F357, and Y547 shown as red stick representation are for comparison

the hydrophobic S1 specificity pocket comprised of residues Tyr547, Tyr631, and Tyr666 via van der Waals interactions; the aromatic ring of isomer SSS could form favorable π-π interaction with the side chain of Phe357; moreover, the amino group and the carbonyl oxygen of caprolactam moiety are involved in the tight hydrogen bonding network in the DPP-IV active site, which is consistent with the co-crystallized observation from the previous publication [16, 17]. Shown in Table 2 is the result of the H-bonding occupancy during MD simulations, the amino group of isomer SSS forms the conserved hydrogen bonds with Glu205/Glu206 (30.25 % and 64.56 %); the carbonyl oxygen of caprolactam moiety forms stable hydrogen bonds with the side chain of Asn710 (75.56 %). It is also worth mentioning that the Arg125 to act as a bridge of Glu205 and Asn710 (55.62 % and 47.56 %) plays an important role in the formation of the tight hydrogen bonding network. From Fig. 6b, it is clear to note the distinction between the binding patterns of isomer SSS and of RRR. The R configuration of chiral center 3* induces a sharp turn of the caprolactam moiety of the inactive isomer RRR, which thus make the caprolactam moiety fail to fully occupy the S1 pocket, but incline to interact with the side chain of Trp629 which is located opposite to Tyr547. Additionally, due to the R configuration of chiral center 11b*, the aromatic ring of isomer RRR is spatially away from the side chain of Phe357, so the favorable π-π interaction between them could not be properly formed. In comparison with the hydrogen bonding network of isomer SSS in the active site, the amino group of isomer RRR forms two weak hydrogen bonds with Glu205/Glu206 (39.69 % and 36.81 %), and the carbonyl oxygen of caprolactam of isomer SSS forms a hydrogen bond with Asn710 (67.81 %); while the Arg125 fails to serve as a bridge in the H-bonding network for the reason that Arg125 moves far away from Glu205 and Asn710, which makes Glu205 and Asn710 not satisfied with the H-bonding interactions. The statistics of H-bonding formation between the other six isomers and the corresponding residues were also performed (in Table S2). It is clear to see that the isomers SSR, RSS, and SRS could form variant percentage of H-bonding interaction with Glu206 (63.00 %, 54.31 %, and 54.89 %, respectively). However, the Arg125 was not engaged in any H-bonding interactions for these three systems, indicating the unstable H-bonding interactions for these three isomers in DPP-IV active site. Although there is H-bonding occupancy of Arg125 for the isomers RSR and RRS (64.38 % and 44.75 %), the H-bonding interactions with Glu206 of these two isomers are relatively weak (30.69 % for isomer RRS) compared to the potent isomer SSS.

Through the above analysis, it can be inferred that the two van der Waals contacts with Tyr547 and Phe357, and the hydrogen bonding interactions with Arg125 and Glu206 are crucial for distinguishing the bioactivity of isomers. Particularly, the failure of Arg125 to act as a bridge in the hydrogen bonding network leads to unstable hydrogen bonding interactions of isomer in DPP-IV active site, which could be the major reason for the bioactivity variance of isomers.

Conclusions

The aminobenzo[a]quinolizine inhibitors were investigated as a novel class of DPP-IV inhibitors. The stereochemistry of this class plays an important role in the bioactivity. In this study, the mechanisms of how different configuration of three chiral centers of the aminobenzo[a]quinolizine inhibitors affects the binding affinity were investigated through molecular dynamics simulations, free energy decomposition analysis. The results indicate that the van der Waals energy contributions and the negative polar desolvation energy are the major reasons for distinct binding affinity of isomers. As to three chiral centers, the S configuration for chiral centers 3* is decisive for isomer to maintain high bioactivity; the chirality effect of chiral center 2* on binding affinity is largely dependent, while

Table 2 Statistics of hydrogen bonds formation between isomers SSS, RRR and the corresponding residues

Inhibitor	Donor	Acceptor	Percentage(%)[a]	Distance(Å)[b]	Angle(°)[c]
(SSS)	:inhibitor@O3	:710@HD21-:710@ND2	75.56	3.043±0.19	19.80±10.51
	:125@NH2	:710@HD22-:710@ND2	47.56	3.218±0.16	49.41±8.78
	:205@OE1	:125@HH21-:125@NH2	55.62	3.117±0.23	42.24±9.43
	:205@OE1	:inhibitor@H9-:inhibitor@N3	30.25	3.345±0.09	49.95±13.96
	:206@OE2	:inhibitor@H9-:inhibitor@N3	64.56	3.109±0.20	19.18±8.38
(RRR)	:inhibitor@O3	:710@HD21-:710@ND2	67.81	3.129±0.19	19.74±10.73
	:205@OE1	:inhibitor@H8-:inhibitor@N3	39.69	3.138±0.22	33.66±14.05
	:206@OE1	:inhibitor@H8-:inhibitor@N3	36.81	3.104±0.19	31.26±12.83

[a] Percentage of snapshots with H-bond formation during MD simulations, percentages lower than 30 % were not shown in the table

[b] Average values and standard deviations of H-bond distance in MD simulation

[c] Average values and standard deviations of H-bond angle in MD simulation

the S configuration for 2* is preferable to R for bioactivity gain; the effect of chiral center 11b* on binding affinity is insignificant. The chirality specificity for three chiral centers is responsible for distinction of two van der Waals contacts with Tyr547 and Phe357, and of H-bonding interactions with Arg125 and Glu206. Particularly, the Arg125 to act as a bridge in the H-bonding network contributes to stable H-bonding interactions of isomer in DPP-IV active site. In brief, it is efficient to investigate the chirality specificity binding mechanisms of inhibitors by combining different molecular modeling techniques. It is expected this work would offer some valuable clues to chiral drug design in the future.

Acknowledgments The project was supported by the National Science Foundation of China (No. 21173264), the Foundation of Knowledge Innovative Engineering of Chinese Academy of Sciences (No. ZNWH-2011-011) and Presidential Foundation of University of Chinese Academy of Sciences (No. Y25101BY00).

References

1. Hussain A, Claussen B, Ramachandran A, Williams R (2007) Prevention of type 2 diabetes: a review. Diabetes Res Clin Pract 76(3):317–326
2. Nathan DM, Buse JB, Davidson MB, Ferrannini E, Holman RR, Sherwin R, Zinman B (2009) Medical management of hyperglycemia in type 2 diabetes: a consensus algorithm for the initiation and adjustment of therapy: a consensus statement of the American Diabetes Association and the European Association for the Study of Diabetes. Diabetes Care 32(1):193–203
3. Ahrrén B (2009) DPP-4 inhibitors. Insulin 4(1):15–31
4. Havale SH, Pal M (2009) Medicinal chemistry approaches to the inhibition of dipeptidyl peptidase-4 for the treatment of type 2 diabetes. Bioorg Med Chem 17(5):1783–1802
5. Kshirsagar AD, Aggarwal AS, Harle UN, Deshpande AD (2011) DPP IV inhibitors: successes, failures and future prospects. Diabetes Metab Syndr Clin Res Rev 5(2):105–112
6. Holst JJ, Deacon CF (2004) Glucagon-like peptide 1 and inhibitors of dipeptidyl peptidase IV in the treatment of type 2 diabetes mellitus. Curr Opin Pharmacol 4(6):589–596
7. Deacon CF (2004) Therapeutic strategies based on glucagon-like peptide 1. Diabetes 53(9):2181–2189
8. Thornberry NA, Gallwitz B (2009) Mechanism of action of inhibitors of dipeptidyl-peptidase-4 (DPP-4). Best Pract Res Clin Endocrinol Metab 23(4):479–486
9. Kim D, Wang L, Beconi M, Eiermann GJ, Fisher MH, He H, Hickey GJ, Kowalchick JE, Leiting B, Lyons K, Marsilio F, McCann ME, Patel RA, Petrov A, Scapin G, Patel SB, Roy RS, Wu JK, Wyvratt MJ, Zhang BB, Zhu L, Thornberry NA, Weber AE (2005) (2R)-4-oxo-4-[3-(trifluoromethyl)-5,6-dihydro[1, 2, 4] triazolo[4,3-a]pyrazin-7(8H)- yl]-1-(2,4,5-trifluorophenyl)butan-2-amine: a potent, orally active dipeptidyl peptidase IV inhibitor for the treatment of type 2 diabetes. J Med Chem 48(1):141–151
10. Deacon CF (2007) Dipeptidyl peptidase 4 inhibition with sitagliptin: a new therapy for type 2 diabetes. Expert Opin Investig Drugs 16(4):533–545
11. Kim SJ, Nian C, Doudet DJ, McIntosh CH (2008) Inhibition of dipeptidyl peptidase IV with sitagliptin (MK0431) prolongs islet graft survival in streptozotocin-induced diabetic mice. Diabetes 57 (5):1331–1339
12. Ahren B (2006) Vildagliptin: an inhibitor of dipeptidyl peptidase-4 with antidiabetic properties. Expert Opin Investig Drugs 15 (4):431–442
13. Villhauer EB, Brinkman JA, Naderi GB, Burkey BF, Dunning BE, Prasad K, Mangold BL, Russell ME, Hughes TE (2003) 1-[[(3-hydroxy-1-adamantyl)amino]acetyl]-2-cyano-(S)-pyrrolidine: a potent, selective, and orally bioavailable dipeptidyl peptidase IV inhibitor with antihyperglycemic properties. J Med Chem 46 (13):2774–2789
14. Feng J, Zhang Z, Wallace MB, Stafford JA, Kaldor SW, Kassel DB, Navre M, Shi L, Skene RJ, Asakawa T, Takeuchi K, Xu R, Webb DR, Gwaltney SL 2nd (2007) Discovery of alogliptin: a potent, selective, bioavailable, and efficacious inhibitor of dipeptidyl peptidase IV. J Med Chem 50(10):2297–2300
15. Pratley RE (2009) Alogliptin: a new, highly selective dipeptidyl peptidase-4 inhibitor for the treatment of type 2 diabetes. Expert Opin Pharmacother 10(3):503–512
16. Boehringer M, Fischer H, Hennig M, Hunziker D, Huwyler J, Kuhn B, Loeffler BM, Luebbers T, Mattei P, Narquizian R, Sebokova E, Sprecher U, Wessel HP (2010) Aryl- and heteroaryl-substituted aminobenzo[a]quinolizines as dipeptidyl peptidase IV inhibitors. Bioorg Med Chem Lett 20(3):1106–1108
17. Mattei P, Boehringer M, Di Giorgio P, Fischer H, Hennig M, Huwyler J, Kocer B, Kuhn B, Loeffler BM, Macdonald A, Narquizian R, Rauber E, Sebokova E, Sprecher U (2010) Discovery of carmegliptin: a potent and long-acting dipeptidyl peptidase IV inhibitor for the treatment of type 2 diabetes. Bioorg Med Chem Lett 20(3):1109–1113
18. Smith RH Jr, Jorgensen WL, Tirado-Rives J, Lamb ML, Janssen PA, Michejda CJ, Kroeger Smith MB (1998) Prediction of binding affinities for TIBO inhibitors of HIV-1 reverse transcriptase using Monte Carlo simulations in a linear response method. J Med Chem 41(26):5272–5286
19. Sham YY, Chu ZT, Tao H, Warshel A (2000) Examining methods for calculations of binding free energies: LRA, LIE, PDLD-LRA, and PDLD/S-LRA calculations of ligands binding to an HIV protease. Proteins 39(4):393–407
20. Kollman P (1993) Free energy calculations: applications to chemical and biochemical phenomena. Chem Rev 93(7):2395–2417
21. DiCapua FM, Beveridge DL (1989) Free energy via molecular simulation: applications to chemical and biomolecular systems. Annu Rev Biophys Biophys Chem 18:431–492
22. Wang J, Hou T, Xu X (2006) Recent advances in free energy calculations with a combination of molecular mechanics and continuum models. Curr Comput Aided Drug Des 2(3):287–306
23. Kollman PA, Massova I, Reyes C, Kuhn B, Huo S, Chong L, Lee M, Lee T, Duan Y, Wang W, Donini O, Cieplak P, Srinivasan J, Case DA, Cheatham TE (2000) Calculating structures and free energies of complex moleculesy molecular mechanics and continuum models. Acc Chem Res 33(12):889–897
24. Gohlke H, Case DA (2004) Converging free energy estimates: MM-PB(GB)SA studies on the protein–protein complex Ras–Raf. J Comput Chem 25(2):238–250
25. Hou T, McLaughlin W, Lu B, Chen K, Wang W (2006) Prediction of binding affinities between the human amphiphysin-1 SH3 domain and its peptide ligands using homology modeling, molecular dynamics and molecular field analysis. J Proteome Res 5(1):32–43
26. Chen Q, Cui W, Cheng Y, Zhang F, Ji M (2011) Studying the mechanism that enables paullones to selectively inhibit glycogen synthase kinase 3 rather than cyclin-dependent kinase 5 by molecular dynamics simulations and free-energy calculations. J Mol Model 17(4):795–803
27. SYBYL molecular simulation package. (2004) http://www.sybyl.com
28. Case DA, Cheatham TE, Darden T, Gohlke H, Luo R, Merz KM, Onufriev A, Simmerling C, Wang B, Woods RJ (2005) The Amber biomolecular simulation programs. J Comput Chem 26(16):1668–1688

29. Duan Y, Wu C, Chowdhury S, Lee MC, Xiong G, Zhang W, Yang R, Cieplak P, Luo R, Lee T, Caldwell J, Wang J, Kollman P (2003) A point-charge force field for molecular mechanics simulations of proteins based on condensed-phase quantum mechanical calculations. J Comput Chem 24(16):1999–2012
30. Wang J, Wolf RM, Caldwell JW, Kollman PA, Case DA (2004) Development and testing of a general amber force field. J Comput Chem 25(9):1157–1174
31. Frisch MJ, Trucks GW, Schlegel HB, Scuseria GE, Robb MA, Cheeseman JR, Montgomery JA, Vreven T, Kudin KN, Burant JC, Millam JM, Iyengar SS, Tomasi J, Barone V, Mennucci B, Cossi M, Scalmani G, Rega N, Petersson GA, Nakatsuji H, Hada M, Ehara M, Toyota K, Fukuda R, Hasegawa J, Ishida M, Nakajima T, Honda Y, Kitao O, Nakai H, Klene M, Li X, Knox JE, Hratchian HP, Cross JB, Bakken V, Adamo C, Jaramillo J, Gomperts R, Stratmann RE, Yazyev O, Austin AJ, Cammi R, Pomelli C, Ochterski JW, Ayala PY, Morokuma K, Voth GA, Salvador P, Dannenberg JJ, Zakrzewski VG, Dapprich S, Daniels AD, Strain MC, Farkas O, Malick DK, Rabuck AD,Raghavachari K, Foresman JB, Ortiz JV, Cui Q, Baboul AG, Clifford S, Cioslowski J, Stefanov BB, Liu G, Liashenko A, Piskorz P, Komaromi I, Martin RL, Fox DJ, Keith T, Laham A, Peng CY, Nanayakkara A, Challacombe M, Gill PMW, Johnson B, Chen W, Wong MW, Gonzalez C, Pople JA (2003) Gaussian 03, revision C.02
32. Bayly CI, Cieplak P, Cornell W, Kollman PA (2003) A well-behaved electrostatic potential based method using charge restraints for deriving atomic charges: the RESP model. J Phys Chem 97:10269–10280
33. Jorgensen WL, Chandrasekhar J, Madura JD, Impey RW, Klein ML (1983) Comparison of simple potential functions for simulating liquid water. J Chem Phys 79:926–935
34. Berendsen HJC, Postma JPM, van Gunsteren WF, DiNola A, Haak JR (1984) Molecular dynamics with coupling to an external bath. J Chem Phys 81:3684–3690
35. Ryckaert JP, Ciccotti G, Berendsen HJC (1977) Numerical integration of the cartesian equations of motion of a system with constraints: molecular dynamics of n-alkanes. J Comput Phys 23:327–341
36. Darden T, York D, Pedersen L (1993) Particle mesh Ewald: an N [center-dot] log(N) method for Ewald sums in large systems. J Chem Phys 98:10089–10092
37. Onufriev A, Bashford D, Case DA (2004) Exploring protein native states and large-scale conformational changes with a modified generalized born model. Proteins 55(383–394)
38. Weiser J, Shenkin PS, Still WC (1999) Approximate atomic surfaces from linear combinations of pairwise overlaps (LCPO). J Comput Chem 20:217–230